Preemptive SOD1 Silencing via Neonatal Intramuscular AAV Therapy Modifies Disease Trajectory in an ALS Mouse Model

Xueqi Gong[1,2,3], Yecheng Xie[4], Wenyuan Wang[5,6*], Tonghui Xu[1,2,3*]

[1]Laboratory Animal Center, Fudan University, Shanghai 200433, China.

[2]Laboratory Animal Resource Center, Fudan University, Shanghai 200433, China.

[3]School of Life Sciences, Fudan University, Shanghai 200438, China.

[4]Department of Neurology, Children's Hospital, Zhejiang, University School of Medicine, National Clinical Research, Center for Child Health, Hangzhou 310052, China

[5]Interdisciplinary Research Center on Biology and Chemistry, Shanghai Institute of Organic Chemistry, Chinese academy of Science, Shanghai 200032, China.

[6]Department of Rehabilitation Medicine, Huashan Hospital, Fudan University, Shanghai 200040, China.

*Corresponding authors: Tonghui Xu, Ph.D. Laboratory Animal Center, Fudan University, Shanghai 200433, China. E-mail: xu_tonghui@fudan.edu.cn.

Wenyuan Wang, Ph.D. Interdisciplinary Research Center on Biology and Chemistry, Shanghai Institute of Organic Chemistry, Chinese academy of Science, Shanghai 200032, China. E-mail: wywang@sioc.ac.cn.

Abstract

Amyotrophic lateral sclerosis (ALS) is a progressive and fatal neurodegenerative disorder with limited therapeutic options. Mutations in the gene encoding superoxide dismutase 1 (*SOD1*) represent a major genetic cause of familial ALS, driving motor neuron degeneration through toxic gain-of-function mechanisms. Although gene silencing approaches targeting *SOD1* show substantial therapeutic potential, their clinical translation remains restricted by suboptimal delivery to the spinal motor neurons and safety concerns linked to conventional viral vectors. This study presents a minimally invasive gene therapy strategy that combines the retrograde transport capability of rAAV2-retro with the safety of an artificial microRNA (miRNA) to achieve pan-spinal *SOD1* silencing. A single intramuscular injection of rAAV2-retro-miRNA into neonatal *SOD1*^{G93A} mice resulted in widespread transduction of spinal motor neurons, significant reduction of mutant SOD1 protein, and multifaceted therapeutic benefits. Treated mice exhibited delayed disease onset, extended lifespan, preserved motor function, reduced neuroinflammation, and protection of neuromuscular junctions and spinal motor neurons. Importantly, the artificial miRNA construct demonstrated a superior safety profile relative to short hairpin RNA (shRNA)-based constructs, which induced marked toxicity and lethality in wild-type mice. These findings establish neonatal intramuscular delivery of rAAV2-retro-miRNA as a safe, efficient, and clinically translatable strategy for preemptive intervention in *SOD1*-mediated ALS, offering broader applicability to other motor neuron diseases.

Introduction

Amyotrophic lateral sclerosis (ALS) is a progressive and fatal neurodegenerative disorder characterized by the selective and sequential degeneration of upper motor neurons in the cerebral cortex and lower motor neurons in the brainstem and spinal cord.[1] Despite significant research efforts, the precise molecular etiology of ALS remains unknown. Clinically, the disease manifests with the insidious onset of muscle weakness progressing to paralysis, resulting in respiratory failure and death typically within 2-5 years of symptom onset. The multifactorial pathophysiology of ALS encompasses a complex interplay of converging mechanisms, including dysregulated RNA metabolism, aberrant protein homeostasis, impaired nucleo-cytoplasmic transport, defective axonal trafficking, mitochondrial dysfunction with concomitant oxidative stress, glutamate-mediated excitotoxicity, and chronic neuroinflammation.[2] Due to the lack of identified therapeutic targets, current management is largely palliative, focusing on symptomatic control and ventilatory support.[3,4] Pharmacological interventions such as riluzole, edaravone (Radicava), and sodium phenylbutyrate-taurursodiol modestly delay disease progression by attenuating glutamatergic transmission or mitigating oxidative stress, but their overall clinical efficacy remains limited.[4-6]

Approximately 10% of ALS cases are familial, reflecting a strong genetic contribution, with identified mutations accounting for about 70% of familial cases.[7] Among these, mutations in genes encoding superoxide dismutase 1 (*SOD1*),[8] TAR DNA-binding protein 43 (*TDP-43*),[9,10] fused in sarcoma (FUS),[11,12] and the C9ORF72 hexanucleotide repeat expansion,[13,14] represent the principal molecular drivers of familial ALS. *SOD1* mutations were the first to be identified and remain among the most extensively studied genetic causes.[8,15-17] Recently, tofersen, an FDA-approved antisense oligonucleotide (ASO) targeting SOD1, achieved up to 36% reduction in the cerebrospinal fluid (CSF) SOD1 protein levels at the highest tested dose,[18,19] underscoring the therapeutic feasibility of gene-targeted approaches in ALS. Although its long-term clinical benefit remains to be fully established, given the limited trial cohort,[18] this milestone approval provides compelling validation for molecular therapies that modulate pathogenic gene expression. In this context, gene therapy has emerged as a transformative paradigm for ALS treatment, aiming to deliver functional genes, neuroprotective factors, or agents to silence the expression of pathogenic genes.

In the context of gene therapy for neurodegenerative disorders such as ALS, adeno-associated virus (AAV) vectors have emerged as the principal gene delivery platforms owing to their favorable safety profile, minimal immunogenicity, and ability to sustain long-term transgene expression across cell populations within the central nervous system (CNS).[20,21] This inherent tropism for neural tissue enables the precise implementation of gene silencing strategies (therapeutic interventions designed to selectively suppress pathogenic alleles at their molecular origin). In the context of ALS gene therapy, the high transduction efficiency of AAV vectors in neural cells makes them particularly well-suited for delivering gene-silencing constructs that target mutant cytosolic *SOD1*, a well-established genetic driver of ALS pathogenesis and a central focus of therapeutic innovation.[8,15-17] To achieve targeted gene silencing, small noncoding RNAs are increasingly employed as therapeutic effectors, with short hairpin RNAs (shRNAs) and artificial microRNAs (miRNAs) representing the most effective molecular modalities. Although both RNA species mediate potent gene suppression, artificial miRNAs offer distinct advantages due to their superior biosafety and reduced cytotoxic potential, making them particularly suitable for chronic neurodegenerative diseases such as ALS, where sustained therapeutic effects are essential.[22,23]

Achieving efficient and sustained transgene expression within disease-relevant neural compartments, particularly spinal motor neurons spanning the lumbar, thoracic, and cervical segments, remains a principal challenge in ALS gene therapy. Current delivery modalities, including intracerebroventricular (ICV), intrathecal (IT), spinal subpial, and intraparenchymal injections, are constrained by significant translational barriers. These invasive neurosurgical techniques necessitate specialized instrumentation, pose procedural postoperative risks, and raise considerable clinical safety concerns. In contrast, intramuscular (IM) administration presents a more clinically practical and less invasive alternative. However, prior studies administering AAV-encoded neuroprotective factors (such as IGF1, IGF2, and HGF) via IM routes have yielded only modest therapeutic efficacy in *SOD1*^{G93A} models, likely attributable to suboptimal transduction efficiency of spinal motor neurons.[24-28] Notably, direct silencing of mutant SOD1 through IM administration remains unexplored and unvalidated in therapeutic contexts. Therefore, advancing clinically viable ALS gene therapies necessitates strategies

that effectively integrate extensive neuraxial distribution with minimally invasive techniques and reduced vector doses.

To overcome the limitations associated with current CNS delivery approaches, this study developed a novel gene-silencing paradigm employing rAAV2-retro vectors administered via IM injection in the *SOD1*^{G93A} transgenic mouse model of ALS. Our prior work demonstrated that a single IM injection of rAAV2-retro into neonatal mice enables widespread transduction of motor neurons across the spinal cord and brainstem motor nuclei, conferring three principal advantages for motor neuron-targeted therapy: (1) highly efficient retrograde transduction of lower motor neurons; (2) minimally invasive peripheral delivery; and (3) intrinsic tropism for motor neurons, minimizing off-target effects.[29] Based on this robust delivery platform, this study hypothesized that a single neonatal IM injection of rAAV2-retro encoding an artificial miRNA could achieve pan-spinal silencing of the mutant gene, thereby delaying disease onset and extending survival in *SOD1*^{G93A} mice**.** The *SOD1*^{G93A} model, which constitutively expresses mutant human SOD1 protein, [30] recapitulates core ALS pathophysiology, including progressive motor neuron degeneration, paralysis, and premature death, rendering it a well-validated platform to test this hypothesis. The present study demonstrates that this strategy achieves extensive spinal cord transduction and robust SOD1 suppression, resulting in significant delay of disease onset, preservation of motor function, attenuation of neuropathological features, and prolonged survival. By overcoming conventional CNS delivery barriers through a minimally invasive peripheral route, this approach addresses a critical unmet need in ALS gene therapy and establishes a clinically translatable platform for targeted silencing strategies.

Results

rAAV2-Retro-Mediated Delivery of an Artificial miRNA Targeting Human SOD1 Enables Efficient Spinal Cord Transduction and Robust Gene Silencing in *SOD1* ^{G93A} Mice.

To establish a novel gene therapy strategy for ALS, the efficiency of delivering an artificial miRNA targeting human *SOD1* to the spinal cord was evaluated using IM injection of rAAV2-retro in *SOD1* ^{G93A} mice. This approach takes advantage of the strong retrograde transport capability of rAAV2-retro, enabling effective transduction of spinal motor neurons through a minimally invasive route to target CNS.[29] An artificial miRNA was engineered on the human miR-30a scaffold, as previously described,[31] exhibiting full complementarity to human SOD1 mRNA and containing at least four base mismatches with murine SOD1 to ensure species-specific silencing (Figure 1A). This miRNA expression cassette, along with an eGFP reporter gene, was cloned into the rAAV2-retro vector under the control of a CAG promoter (designated rAAV2-retro-miRNA). A control vector expressing a scrambled miRNA sequence (rAAV2-retro-Scramble) was generated in parallel.

To evaluate the silencing efficacy, *SOD1* ^{G93A} mice (n = 4) received bilateral IM co-injections of rAAV2-retro-miRNA into the extensor carpi radialis (forelimb) and gastrocnemius (hindlimb) muscles at postnatal day 4 (P4; 1 μL per site, 1.0×10^{13} GC/mL). Four weeks post-injection, Western blot analysis of lumbar spinal cord lysates demonstrated a significant reduction (47.2%)

in human SOD1 protein levels compared to rAAV2-retro-Scramble-treated animals (Figures 1B and 1C). The expression of endogenous murine SOD1 mRNA remained unchanged (Figure S1), confirming its specificity for the human transgene.

Following confirmation of target knockdown, the therapeutic potential of this strategy was assessed. *SOD1* ^{G93A} mice of both sexes were treated at P4 with IM injections of either rAAV2-retro-miRNA or rAAV2-retro-Scramble (1 μL per muscle, 1.0×10^{13} GC/mL). Longitudinal evaluations included disease onset (defined by peak body weight decline), survival, motor performance (rotarod, grip strength, open-field tests), and neurological signs (limb clasping). Terminal electrophysiological (CMAP) and histological analyses were conducted at 130 days of age (Figure 1D).

The biosafety of the artificial miRNA construct was compared with that of a conventional shRNA approach in wild-type mice. Neonates were administered with IM injections of either rAAV2-retro-miRNA or rAAV2-retro-shRNA at P4. While the artificial miRNA construct exhibited no adverse effects on body weight or survival, delivery of the shRNA construct resulted in significant weight loss within one week and uniform lethality by three weeks post-injection (Figure S2). This dramatic difference underscores the superior safety profile of the artificial miRNA platform, supporting its translational potential for therapeutic applications in the CNS.

Intramuscular Delivery of rAAV2-Retro-miRNA Significantly Delays Disease Onset and Extends Survival in *SOD1*^{G93A} Mice.

To assess the therapeutic efficacy of rAAV2-retro-mediated SOD1 silencing, disease progression in treated *SOD1*^{G93A} mice was longitudinally monitored by measuring body weight and survival until the humane endpoint (Figure 2 and Figure S3). Disease onset was defined as the age at which animals sustained a 10% loss from their peak body weight. Remarkably, rAAV2-retro-miRNA treatment significantly delayed disease onset by 38 days compared to scramble-injected controls (median onset: 171.5 vs. 133.5 days; $P < 0.0001$; Figure 2A). Moreover, miRNA-treated mice exhibited a pronounced extension in median survival, living 61 days longer than scramble-injected control animals (median survival: 216 days vs. 155 days; $P < 0.0001$; Figures 2B and 2C).

Further analysis of disease phases revealed that the early disease period (from peak weight to 10% weight loss) was significantly prolonged in miRNA-treated mice (67.08 days vs. 49.00 days in controls; $P = 0.0188$; Figure 2D). Similarly, the late disease phase, defined as the interval between 10% weight loss and endpoint, was significantly lengthened (25.67 days vs. 16.33 days; $P = 0.0351$; Figure 2E). Consequently, the total disease duration was substantially increased in the rAAV2-retro-miRNA group (92.75 days) relative to the scramble control group (65.33 days; $P = 0.0005$; Figure 2F). These results demonstrate that a single neonatal IM injection of rAAV2-retro-miRNA markedly delays disease progression and improves survival in this ALS model.

Intramuscular Delivery of rAAV2-Retro-miRNA Preserves Motor Function in *SOD1*^{G93A} Mice.

To assess neuromuscular integrity comprehensively, a longitudinal behavioral analysis was

conducted beginning at postnatal day 60. The experimental battery included rotarod, grip strength, open-field, and limb clasping assays, all conducted by investigators blinded to the treatment groups. Administration of rAAV2-retro-miRNA markedly preserved motor function. By 18 weeks, open-field locomotor activity declined by only 33.9% in miRNA-treated mice, compared to a 75.74% reduction observed in scramble controls (Figure 3A). Notably, by day 135, all scramble-treated mice exhibited dystonic limb clasping, whereas one-third of miRNA-treated animals remained completely free of this neurological sign (Figure 3B). Furthermore, miRNA-treated mice demonstrated significantly enhanced motor coordination on the rotarod and maintained higher forelimb and hindlimb grip strength compared to scramble controls (Figures 3C and 3D). Collectively, these findings demonstrate that rAAV2-retro-miRNA treatment sustains motor function and muscle strength over prolonged disease progression.

rAAV2-Retro-miRNA Gene Therapy Mitigates Neuromuscular Junction Denervation and Muscle Atrophy in *SOD1*^{G93A} Mice.

To evaluate the protective effects of rAAV2-retro-miRNA on the integrity of neuromuscular junction (NMJ) and muscle morphology, NMJs and myofibers were systematically analyzed. Consistent with the progressive pathology of ALS, only 10.12% of NMJs remained fully innervated in scramble-treated *SOD1*^{G93A} mice by day 130, with the majority exhibiting partial or complete denervation (Figures 4A and 4B). In contrast, neonatal administration of rAAV2-retro-miRNA significantly preserved NMJ innervation and mitigated denervation.

Given the critical role of NMJ integrity in maintaining muscle mass, myofiber CSA was quantified using laminin immunostaining. Scramble-treated *SOD1*^{G93A} mice displayed pronounced muscle atrophy, with a mean CSA (765.7 μm²) significantly smaller than that observed in wild-type mice (3009 μm²; P = 0.0008; Figures 4C and 4D). Treatment with rAAV2-retro-miRNA markedly attenuated atrophy, increasing mean CSA to 2090 μm² (P = 0.0038 *vs.* scramble; Figures 4C and 4D), and preventing whole-muscle mass loss (Figure S4).

Functional assessment of NMJ transmission at 130 days revealed significantly higher CMAP amplitudes in rAAV2-retro-miRNA-treated mice compared to scramble controls (Figures 4E and 4F), indicating improved neuromuscular transmission and delayed functional denervation. Collectively, these results demonstrate that rAAV2-retro-miRNA therapy effectively preserves NMJ innervation, alleviates muscle atrophy, and maintains electrophysiological function in *SOD1*^{G93A} mice.

Intramuscular Delivery of rAAV2-Retro-miRNA Preserves Spinal α-motoneurons and Suppresses Mutant SOD1 Expression in *SOD1*^{G93A} Mice.

Degeneration of spinal motor neurons and skeletal muscle denervation represent key pathological hallmarks of ALS. Immunohistochemical analyses revealed severe loss of α-motoneurons across all spinal cord segments in scramble-treated *SOD1*^{G93A} mice at day 130, compared to wild-type controls. In contrast, treatment with rAAV2-retro-miRNA significantly preserved α-motoneuron survival throughout the spinal cord (Figures 5A and 5B).

Quantitative analysis demonstrated that scramble-treated *SOD1*^{G93A} mice exhibited a decline in NeuN□ neuronal count to roughly 50% of wild-type levels (cervical: 55.44%; thoracic: 57.44 %; lumbar: 48.94%), whereas rAAV2-retro-miRNA treatment maintained NeuN□ neurons above 70% of normal values (cervical: 76.16%; thoracic: 74.49%; lumbar: 70.32%). Consistent with these neuroprotective effects, pronounced human SOD1 (hSOD1) immunoreactivity was observed in the spinal cord of scramble-treated *SOD1*^{G93A} mice, while rAAV2-retro-miRNA administration markedly suppressed hSOD1 expression (Figures 5C and 5D).
Collectively, these findings demonstrate that neonatal IM delivery of rAAV2-retro-miRNA effectively downregulates mutant SOD1 levels and provides broad neuroprotection across the spinal cord.

Intramuscular Delivery of rAAV2-Retro-miRNA Attenuates Neuroinflammation in the Spinal Cord of *SOD1*^{G93A} Mice.

Neuroinflammation, characterized by the activation of microglia and astrocytes, is a prominent pathological hallmark of ALS. To determine whether rAAV2-retro-miRNA treatment modulates neuroinflammatory response, immunofluorescence analyses were performed on spinal cord sections. Treatment with rAAV2-retro-miRNA markedly reduced the fluorescence intensity of both Iba1 (microglia) and GFAP (astrocytes) relative to scramble-injected *SOD1*^{G93A} controls (Figure 6), indicating suppression of glial activation. These results demonstrate that targeted silencing of mutant SOD1 via rAAV2-retro-miRNA not only preserves motor neurons but also attenuates neuroinflammation in this ALS model.

Discussion

This study establishes a minimally invasive and effective gene therapy approach that integrates the enhanced retrograde transport capability of rAAV2-retro with the safety and precision of an artificial miRNA platform to achieve targeted silencing of the human SOD1 gene. A single IM administration of rAAV2-retro-miRNA in neonatal *SOD1*^{G93A} mice led to widespread transgene expression throughout the spinal cord, significant suppression of mutant SOD1 protein, and a broad spectrum of therapeutic benefits, including delayed disease onset, extended lifespan, improved motor function, and preservation of NMJs and spinal motor neurons. This approach effectively overcomes major delivery challenges associated with conventional CNS-directed gene therapies, providing a novel foundation for early, pre-symptomatic intervention in inherited ALS.

The present study demonstrates several technological advances: First, the application of rAAV2-retro, a vector exhibiting superior retrograde transduction efficiency in neonatal animals, circumvents the limited spinal cord transduction observed with conventional AAV serotypes in adults. Neonatal IM administration of rAAV2-retro-CAG-miRNA achieved

robust and widespread gene silencing across spinal motor neurons, surpassing the restricted, region-specific expression profiles reported in prior studies.

Second, in contrast to single neurotrophic factor therapies, this approach employs miRNA-mediated *SOD1* gene silencing, thereby preventing the accumulation of toxic protein aggregates and mitigating downstream pathogenic mechanisms such as mitochondrial dysfunction and neuroinflammation. This *"upstream interception*" strategy targets the core pathology of ALS, offering a mechanistic advantage over neuroprotective interventions that primarily enhance neuronal survival without addressing the underlying cause.

Third, leveraging the immunological immaturity of neonatal mice and the genomic stability of rAAV2-retro, a single IM dose establishes long-term therapeutic expression and sustained efficacy throughout postnatal development. This approach substantially reduces the need for repeated interventions in adulthood, which are often constrained by the mature blood-brain barrier (BBB) and heightened immune surveillance. Consequently, this neonatal gene delivery via rAAV2-retro represents a foundational therapy with unique translational advantages in ALS.

This study establishes a developmental early intervention paradigm that, for the first time, achieves pan-spinal precision-targeted *SOD1* gene silencing in pre-symptomatic *SOD1*^{G93A} neonatal mice. This intervention effectively disrupts the pathogenic feed-forward loop between neuroinflammation and NMJ degeneration, thereby markedly delaying ALS pathological progression and prolonging lifespan. The finding aligns with the seminal AAV10-U7 study,[32] in which combined intracerebroventricular and intravenous (ICV/IV) administration at postnatal day 1 significantly extended median survival, validating the critical therapeutic window for pre-symptomatic intervention in *SOD1*-mediated ALS. These results have broad scientific and translational implications. Notably, the SO*D1* mutation, a central genetic driver of familial ALS, initiates pathogenic processes as early as embryonic development.[33] Critically, *SOD1*^{G93A} mice demonstrate subclinical pathology, such as motor neuron hyperexcitability, shortly after birth; however, these early pathogenic processes remain concealed by compensatory mechanisms that delay the manifestation of clinical symptoms for several months.[17] The present intervention targets this pre-symptomatic window, prior to the age-dependent failure of compensatory mechanisms and the theoretical point-of-no-return in neurodegeneration, thereby maximizing the therapeutic efficacy of SOD1 silencing by mitigating toxicity at its origin.

Second, during the neonatal period, prior to the onset of motor neuron synaptic stripping[34] and while the complement system remains immature,[35] leveraging the transiently high permeability of the BBB[36] enables highly efficient CNS transduction via IM injection of rAAV2-retro. This approach achieves broad SOD1 gene silencing across spinal motor neurons, thereby attenuating the toxic accumulation of misfolded SOD1 protein and

interrupting the downstream molecular cascade involving mitochondrial dysfunction, glial cell activation, and excitotoxicity.[37]

Third, the immaturity of the neonatal immune system significantly diminishes adaptive immune responses against both the viral capsid and the transgene product, thereby promoting sustained and stable transgene expression. In contrast to the adult-stage interventions, which require high doses or invasive procedures due to a mature BBB and heightened immune surveillance, this approach underscores the distinct therapeutic advantage of early intervention in ALS gene therapy.

Fourth, these findings establish a conceptual framework for newborn screening and preemptive intervention in high-risk *SOD1*-ALS families. The proposed approach integrates early genetic identification of *SOD1* mutation carriers with pre-symptomatic administration of gene therapy to intercept disease initiation. Such early intervention is anticipated to markedly reduce the lifetime healthcare burden associated with ALS, offering significant cost-effectiveness advantages. Implemented during a developmental window of heightened neuroplasticity, this paradigm transcends the therapeutic focus from traditional "post-damage repair" to proactive neuroprotection. Moreover, this framework provides a translatable preventive strategy for other motor neuron disorders and inherited neurological conditions, including spinal muscular atrophy (SMA).

Current gene delivery strategies for ALS, including intrathecal (IT), ICV, or spinal parenchymal (SP) injections, rely on invasive administration routes that require complex medical devices or high-risk surgical procedures. These methods are associated with procedural complexity and substantial clinical risk, thereby limiting their translational feasibility. For example, intrathecal administration requires lumbar puncture, which may lead to complications such as post-procedural headaches, cerebrospinal fluid (CSF) leakage, and infection.[38] Furthermore, intrathecal administration of AAV vectors can activate cytotoxic T lymphocytes (CTLs), triggering neuroinflammatory responses targeting dorsal root ganglia and resulting in neuronal loss and immune cell infiltration.[38] More importantly, preclinical evidence indicates that achieving uniform transduction across the spinal cord via intrathecal delivery necessitates administration of large vector volumes (e.g., administering approximately half the total CSF volume in humans). Such an approach poses substantial safety concerns, as it may induce acute intracranial pressure fluctuations and electrolyte disturbances, resulting in potential neurotoxicity.[39] Collectively, these technical and safety limitations severely restrict the clinical applicability of intrathecal gene delivery. Compared with intrathecal delivery, IM injection offers distinct technical and safety advantages. As a minimally invasive approach, it does not require specialized medical devices or high-risk surgical procedures, thereby reducing procedural complexity and minimizing the likelihood of clinical complications. Studies have shown that IM administration of rAAV vectors enables retrograde axonal transport to spinal motor neurons, resulting in efficient CNS transduction

with limited systemic exposure. For example, in *SOD1*^{G93A} ALS mouse models, IM delivery of AAV6-HGF improved muscle histology, delayed disease progression, and prolonged survival.[28] Similarly, IM delivery of AAV9-IGF2 not only preserved motor neurons but also promoted axonal regeneration.[26] Collectively, these findings underscore the targeting specificity, low invasiveness, and durable therapeutic efficacy of IM injection, supporting its potential as a promising delivery platform for ALS gene therapy.

Our study advances this therapeutic paradigm through several key innovations. First, the approach utilizes a substantially lower viral dose compared with conventional AAV studies, reducing production costs without compromising therapeutic efficacy. Second, intervention at postnatal day 4 (P4) (during the very early pre-symptomatic stage) enables earlier disruption of pathogenic processes than most established protocols. Third, unlike systemic IV delivery, which requires extremely high vector doses to achieve only partial spinal transduction, our IM strategy ensures efficient and neuron-selective targeting of spinal motor neurons. This feature effectively overcomes the dose-dependent limitations and safety concerns associated with IV administration.

Mechanistically, our strategy represents a fundamental departure from prior IM studies. Earlier approaches primarily delivered neurotrophic factors (e.g., IGF-1, IGF-2, HGF) via IM injection to ameliorate pathology. While beneficial, these approaches offer modest efficacy due to their single-mechanism, symptomatic focus.[24-26,28] In contrast, the present study employs rAAV2-retro-mediated *SOD1* gene silencing during the neonatal period, directly addressing the genetic etiology of ALS. This causal intervention disrupts the pathogenic cascade at its origin, yielding multidimensional therapeutic benefits, including improved motor function, enhanced motor neuron survival, reduced apoptosis and neuroinflammation, preserved NMJs, and mitigation of muscle atrophy. The scope of this assessment exceeds that of most prior studies. Collectively, the findings validate that targeted genetic silencing can comprehensively ameliorate core ALS pathologies, establishing the broad efficacy of causal gene-targeting therapies.

Mutations in the superoxide dismutase 1 (*SOD1*) gene account for approximately 20% of familial ALS cases, with over 150 pathogenic variants identified to date.[40] Substantial evidence indicates that *SOD1* mutations contribute to ALS pathogenesis through multiple, interrelated mechanisms. A prevailing hypothesis posits that mutant *SOD1* acquires toxic gain-of-function properties, resulting in protein misfolding and aggregation, a histopathological hallmark of *SOD1*-linked ALS.[41,42] Notably, misfolded *SOD1* inclusions have also been detected in a subset of sporadic ALS cases, suggesting that SOD1-targeted therapeutic strategies could have broader clinical applicability beyond familial disease.[43,44] Although the precise mechanistic cascade remains incompletely elucidated, converging evidence supports that SOD1-mediated toxicity perturbs critical cellular functions,

collectively driving motor neuron degeneration.[45,46] Consequently, suppression of mutant SOD1 expression represents a rational therapeutic strategy. Preclinical studies have consistently demonstrated that silencing mutant *SOD1* prolongs survival, delays symptom onset, and preserves motor function in ALS rodent models, thereby establishing SOD1 as a leading target for gene therapy development.[47] Unlike neurotrophic support strategies (e.g., IGF1, BDNF) that modulate downstream consequences of neurodegeneration, direct *SOD1* silencing intervenes at the primary pathogenic source.[17] As the first genetically defined form of ALS, *SOD1* has been extensively investigated in AAV-RNAi-based interventions, with progressive refinement of therapeutic efficacy.[48] This study significantly advances this paradigm by introducing a clinically translatable rAAV2-retro IM platform that enables efficient and widespread motor neuron transduction in neonatal animals. Moreover, this strategy is readily adaptable for targeting other ALS-linked genes (e.g., *C9orf72, FUS, TARDBP*)[49] or motor neuron disease-associated mutations, offering a versatile clinical platform for MN diseases.

In this study, the artificial miRNA sequence targeting human SOD1 was delivered via rAAV2-retro by neonatal IM injection, achieving robust gene silencing and therapeutic efficacy. Notably, parallel experiments in wild-type mice demonstrated that rAAV2-retro-mediated delivery of shRNA constructs induced rapid weight loss and uniform lethality within three weeks post-injection, highlighting the acute toxicity associated with shRNA-based approaches. This striking contrast emphasizes the superior safety profile of artificial miRNAs compared with shRNAs in CNS-directed gene therapy.

While both utilize RNA-induced silencing complex (RISC) for silencing, shRNAs (Pol III-driven, perfect complementarity) can oversaturate the RNAi pathway by competing for Exportin-5, leading to global microRNA dysfunction and acute toxicity. This mechanism aligns with neonatal lethality observed in the present study and previous reports.[50] In contrast, artificial miRNAs (Pol II-driven, engineered mismatches) recapitulate endogenous pri-miRNA processing, thereby minimizing RISC saturation while preserving target specificity.[17] While potential cardiotoxic effects from muscle-directed RNAi cannot be fully excluded, the rapid lethality and rAAV2-retro's neuronal tropism suggest that acute neuronal RNAi dysregulation is the dominant pathological mechanism.[51] Collectively, these findings validate the superior safety profile of engineered miRNAs over shRNAs, underscoring their critical advantage for clinical translation in ALS gene therapy.

Our study establishes a foundational therapeutic framework by demonstrating that neonatal IM delivery of rAAV2-retro vectors enables preemptive silencing of pathogenic SOD1 at its genetic source, effectively delaying ALS onset and extending survival in transgenic mice. This early intervention creates a platform for subsequent reinforcement or sustained therapeutic intervention. Future directions include designing dual-component vectors that co-deliver SOD1-targeting miRNAs with neuroprotective factors such as IGF1, as well as developing combinatorial regimens integrating neonatal gene silencing with adult-stage

therapies. The pan-spinal motor neuron transduction achieved by rAAV2-retro via IM injection unlocks transformative potential for spinal cord research. Beyond ALS, this platform facilitates precise circuit dissection using Cre/loxP or CRISPR systems, facilitating targeted gene manipulation in models of hereditary spastic paraplegia or spinal muscular atrophy. Integration with optogenetic tools (e.g., ChR2) or chemogenetic systems (e.g., DREADDs) permits real-time functional mapping of motor ensembles involved in locomotion and pain processing, while calcium indicators (e.g., GCaMP) link histological alterations to functional outcomes during disease progression. Therapeutically, the approach supports multi-target interventions that combine neuroprotection, gene silencing, and regeneration to counteract neurodegeneration synergistically. Its minimally invasive delivery enhances clinical feasibility, and continued optimization of vector tropism and immune evasion in large-animal models will accelerate translation toward precision therapies for spinal and motor neuron disorders, advancing innovative paradigms in neuromedicine.

Methods

Animals

C57BL/6J (stock no.000664) and high-copy transgenic *SOD1* ^{G93A} mice [B6. Cg-Tg(*SOD1*^{G93A})/1Gur/J] (stock no.004435) were obtained from The Jackson Laboratory (Bar Harbor, ME, USA). Transgenic littermates of both sexes expressing elevated levels of the mutant *SOD1*^{G93A} transgene were randomly and equally assigned to experimental groups, while non-transgenic littermates served as wild-type controls. All animals were maintained under specific pathogen-free (SPF) conditions in the institutional animal facility with controlled temperature, humidity, light, and noise levels and kept on a 12-hour light/dark cycle with *ad libitum* access to food and water. All experimental procedures were approved by the Animal Experimental Ethics Committee of Shanghai Medical School, Fudan University, China, and were performed in accordance with the institutional guidelines.

Production, Purification, and Titration of Recombinant AAV Vectors

A single-stranded recombinant AAV2-retro vector was engineered to express enhanced green fluorescent protein (eGFP) under the control of a CAG promoter. The construct also incorporated a synthetic miRNA sequence designed to target human SOD1 mRNA (exon 2), followed by the woodchuck hepatitis virus post-transcriptional regulatory element (WPRE) and an SV40 polyadenylation (poly(A)) signal. The artificial miRNA, optimized to specifically silence human *SOD1* without cross-reactivity to murine SOD1, was embedded within the human *miR-30a* scaffold, as previously described.[31] The complete oligonucleotide sequence of the artificial miRNA is provided below, with the guide strand underlined:

miR-30a construct:5’-TGTTTGAATGAGGCTTCAGTACTTTACAGAATCGTTGCC
TGCACATCTTGGAAACACTTGCTGGGATTACTTCTTCAGGTTAACCCAACAGAAGGCA
AAGAAGGTATATTGCTGTTGACAGTGAGCG<u>TCATGAACATGGAATCCATG</u>TAGTGAAG
CCACAGATGTAAAGGTGGATGAAGAAAGTATGCCTACTGCCTCGGACTTCAAGGGGCT
ACTTTAGGAGCAATTATCTTGTTTACTAAAACTGAATACCTTGCTATCTCTTTGATACATT
TTTACAAAGCTGAATTAAAATGGTATAAATTAAATCACTTTA-3’.

Recombinant vectors were packaged into AAV2 capsids using a triple-plasmid transfection in HEK 293 cells. The transfection mixture comprised: (1) the AAV2 inverted terminal repeat

(ITR)-based transgene plasmid, (2) a helper plasmid expressing AAV2 *Rep* and *Cap* genes, and (3) the adenoviral helper plasmid pHELP. Subsequently, viral particles were purified, and titers were determined using quantitative PCR (qPCR).

An analogous rAAV2-retro-shRNA vector was generated to express a short hairpin RNA (shRNA) targeting human SOD1 mRNA (exon 2) under the same CAG promoter, followed by an SV40 polyadenylation signal.

Intramuscular Injection

As described previously, cryoanesthesia was induced in postnatal day 4 (P4) mice by briefly placing them on pre-chilled aluminum plates.[29] For IM administration, small incisions were made using fine surgical scissors to expose target muscles (the left flexor carpi ulnaris and the right gastrocnemius). Recombinant AAV vectors were diluted in phosphate-buffered saline (PBS) to a concentration of 1×10^{13} genomic copies (GC)/mL. A total of 2 μL, containing 2×10^{10} GC of each vector, was injected into each muscle using a glass micropipette connected to a high-precision syringe pump (Quintessential Stereo taxic Injector, Model 53311). Injections were administered at a constant rate of 1.0 μL/min. To minimize reflux and ensure complete delivery, the pipette was held in place for 30 seconds following each injection before being slowly withdrawn. After the procedure, pups were allowed to recover on a warming pad before being returned to their home cages.

Western Blot

Mice were deeply anesthetized, decapitated, and tissues were rapidly dissected, snap-frozen in liquid nitrogen, and stored at -80°C. For protein extraction, frozen tissues or cultured cells were homogenized in RIPA buffer (Beyotime, P0013B) supplemented with a protease inhibitor cocktail (Beyotime, ST506). Lysates were mixed with loading buffer (Tsingke, TSJ010) and boiled at 100°C for 10 minutes. Equal amounts of proteins were separated by SDS-PAGE and transferred onto polyvinylidene fluoride (PVDF) membranes. Membranes were blocked with 5% non-fat dry milk in Tris-buffered saline containing 0.05% Tween-20 (TBST; 20 mM Tris-HCl, 150 mM NaCl, pH 7.5) for 1 hour at room temperature, followed by overnight incubation at 4°C with primary antibodies. After washing, membranes were incubated with horseradish peroxidase (HRP)-conjugated secondary antibodies. The following antibodies were used: mouse anti-hSOD1 (1:200, Santa Cruz Biotechnology, sc-17767), mouse anti-Actin (1:5000, Proteintech, 66009-1-IG), mouse anti-eGFP (1:1000, Santa Cruz Biotechnology, sc-5384), and HRP-conjugated goat anti-mouse IgG (1:5000, YEASEN, 33201ES60). Protein bands were visualized using enhanced chemiluminescence, and band intensities were quantified using Image Lab (Bio-Rad) or ImageJ software, normalized to β-Actin levels in each lane.

RNA Extraction, Reverse Transcription, and Quantitative Real-Time PCR

Total RNA was isolated from cultured N2A cells using TRIzol™ Reagent (Thermo Fisher Scientific, 15596018CN) as per the manufacturer's protocol. RNA concentration and purity were determined spectrophotometrically by measuring absorbance at 260 and 280 nm, and integrity was confirmed by the 260/280 nm ratio. Complementary DNA (cDNA) was synthesized from 1 μg of total RNA using random primers and the Hifair® III First Strand cDNA Synthesis Kit (Yeasen Biotechnology, 11141ES60).

qPCR was performed using the 2× SYBR Green qPCR Master Mix (Selleck Chemicals, B21203) on a Bio-Rad iCycler iQ6 Detection System. Each reaction contained cDNA corresponding to 100 ng of total RNA. Amplification parameters followed the manufacturer’s instructions. The human

SOD1 gene was amplified with the following primers:
Forward: 5′-GGGAAGCTGTTGTCCCAAG-3′
Reverse: 5′-CAAGGGGAGGTTAAAAGAGAGC-3′
Mouse GAPDH (NM_001289726.2) served as endogenous control and was amplified with the following primers:
Forward: 5′-CACCATCTTCCAGGAGCGAG-3′
Reverse: 5′-CCTTCTCCATGGTGGTGAAGAC-3′
Relative mRNA expression levels were calculated using the 2^−ΔΔCt method, and data acquisition and analysis were performed with Bio-Rad iQ6 Optical System Software.

Behavioral Analysis

Behavioral assessments were conducted to evaluate disease progression and motor performance in wild-type (WT), rAAV2-retro-Scramble-treated, and rAAV2-retro-miRNA-treated *SOD1* ^{G93A} mice. All tests were performed during the light phase under consistent environmental conditions, and experimenters were blinded to group identity throughout data collection.

Body Weight Measurement: Body weight was recorded weekly beginning at postnatal week 5 and continued until end-stage disease to monitor disease progression.

Rotarod Test: Motor coordination and balance were assessed using an accelerating rotarod apparatus (KEW BASIS, KW-6D). Mice underwent three consecutive trials per session, with the rotation speed gradually increasing from 5 rpm to 40 rpm over a minute. The latency to fall was recorded for each trial.

Limb Clasping Assay: Hindlimb clasping behavior was evaluated at 135 days of age by suspending mice by the tail for 10 seconds with the heads oriented downward. A clasping score was assigned if the behavior persisted for more than 2 seconds using the following criteria: 1 point for unilateral hindlimb clasping, 2 points for bilateral hindlimb clasping, and 3 points if clasping involved both hindlimbs, forelimbs, or torso curling.

Grip-Strength Test: Forelimb and hindlimb grip strength were quantified using a grip-strength meter (KEW BASIS, KW-ZL). Mice were allowed to grasp a horizontal metal bar with either forelimbs or hindlimbs, and were gently pulled backward in a consistent motion until they released the bar. The peak tension (in grams) was recorded over five consecutive trials, and the mean value was calculated for each mouse.

Open-Field Test: Spontaneous locomotor activity was evaluated in a clean, opaque acrylic open-field arena (50 cm × 50 cm) for one hour. Animal movement was recorded and analyzed using EthoVision Video Tracking Software (Noldus). The total distance traveled and movement patterns were used to analyze locomotor activity and exploratory behavior.

Assessment of Disease Progression and Survival

The humane experimental endpoint was defined as the time point at which an animal was unable to right itself within 30 seconds of being placed on its back. Disease onset and progression were evaluated retrospectively based on recorded physiological and behavioral data. Disease onset was defined as the age at which the animal attained its peak body weight. The overall disease duration was calculated as the interval between disease onset and the experimental endpoint. The disease course was further subdivided into two phases: the early phase, extending from peak body weight to a 10% reduction in peak weight, and the late phase, spanning from 10% weight loss threshold to the endpoint.

Compound Muscle Action Potential (CAMP) Measurement

At 130 days of age, mice were anesthetized with isoflurane, and hair from the hindlimb and lower back regions was gently removed using depilatory cream before electrophysiological recording. The stimulating electrode was positioned at the lumbar spinal roots, while the active recording electrode was placed over the belly of the gastrocnemius muscle. The reference electrode was placed near the Achilles tendon or digit of the ipsilateral hindlimb (iWork, IX-RA-834ECG).

Tissue Preparation

Following euthanasia via isoflurane overdose, mice were transcardially perfused with phosphate-buffered saline (PBS) to remove circulating blood, followed by fixation with 4% paraformaldehyde (PFA) in PBS. The perfused tissues were post-fixed in 4% PFA overnight at 4°C. Spinal cords were cryoprotected in 30% sucrose for 24 hours and sectioned at a thickness of 30 μm using a freezing microtome (Leica, CM3050 S). Gastrocnemius muscle and liver tissues were dehydrated, embedded in paraffin, and sectioned into 3 μm slices using a rotary microtome (Leica, 149BIO000C1).

Immunohistochemistry and Histological Analysis

For immunohistochemical staining of spinal cord sections, fixed sections were rinsed three times with PBS and subjected to antigen retrieval using 1× citrate buffer (Sangon Biotech, A100101-0500). Sections were then permeabilized and blocked for one hour at room temperature with 5% goat serum (Sangon Biotech, E510009-0100) and 0.3% Triton X-100 (Beyotime, P0096) in PBS. Following blocking, samples were incubated overnight at 4°C with primary antibodies diluted in PBS containing 3% goat serum (Sangon Biotech, E510009-0100) and 0.1% Triton X-100 (Beyotime, P0096). The following primary antibodies were used: rabbit anti-ChAT (1:1000, Abcam, ab178850), chicken anti-NeuN (1:1000, Millipore, ABN91), mouse anti-eGFP (1:1000, Santa Cruz Biotechnology, sc-5384), rabbit anti-Iba1 (1:1000, Abcam, ab178846), rabbit anti-GFAP (1:1000, Abcam, ab7260), rabbit anti-hSOD1 (1:500, Cell Signaling Technology, 2770).

After washing three times with PBS, sections were incubated for 2 hours at room temperature in the dark with appropriate secondary antibodies: donkey anti-mouse Alexa Fluor 488 (1:500, Thermo Fisher, A-20102), goat anti-chicken Alexa Fluor 647 (1:1000, Abcam, ab150171), and donkey anti-rabbit Alexa Fluor 555 (1:500, Thermo Fisher, A-31572). Nuclei were counterstained with DAPI (1:1000, Sigma-Aldrich, 10236276001) for 10 minutes, followed by three PBS washes. Sections were mounted using antifade mounting medium (SouthernBiotech, 0100-01) prior to imaging.

For immunohistochemical staining of liver sections, paraffin-embedded liver tissues were deparaffinized in xylene (Sinopharm Chemical Reagent, 10023428) and rehydrated through a graded ethanol series (Sinopharm Chemical Reagent, 100092680). Antigen retrieval was performed using microwave heating in Tris-EDTA buffer (Solarbio, C1038). Sections were then blocked with 5% normal goat serum for 1 hour at room temperature and incubated overnight at 4°C with the following primary antibody: mouse anti-eGFP (1:1000, Santa Cruz Biotechnology, sc-5384). Following three washes with TBS-T, slides were incubated for 1–2 hours at room temperature in the dark with the corresponding secondary antibody: donkey anti-mouse Alexa Fluor 488 (1:500, Thermo Fisher Scientific, A-20102). Nuclei were counterstained with DAPI (1:1000, Sigma-Aldrich, 10236276001) for 10 minutes, washed with TBS-T, and mounted with antifade mounting medium (SouthernBiotech, 0100-01) for subsequent imaging.

For NMJ immunostaining, gastrocnemius muscles were dissected and teased into small bundles

containing 2-3 fibers, as previously described[52]. Muscle bundles were incubated with chicken anti-neurofilament (1:2500, Abcam, ab4680) to label presynaptic axons and fluorophore-conjugated α-bungarotoxin (α-BTX, Biotium, 00018) to identify postsynaptic acetylcholine receptors.

For H&E Staining, paraffin-embedded gastrocnemius muscle sections were deparaffinized in xylene (Sinopharm Chemical Reagent, 10023428) and rehydrated through a graded ethanol series (Sinopharm Chemical Reagent, 100092680). Nuclei were stained with Harris hematoxylin (Beyotime, C0107) for 5 minutes, rinsed under tap water, and differentiated in 1% acid alcohol (Beyotime, C0163M). Sections were blued in Scott's tap water substitute and counterstained with eosin (Beyotime, C0109) for 1 minute. After dehydration and xylene clearing, slides were mounted with a resinous medium (Sangon, E675007) for histopathological evaluation.

Fluorescence Microscopy and Imaging Analysis

Spinal cord and liver sections were initially scanned using a high-resolution digital slide scanner (PANNORAMIC 250 Flash III, 3DHISTECH) equipped with a 20× objective lens. Representative high-magnification images were acquired using a Leica SP8 confocal microscope with a 40× oil-immersion objective. Z-stack images were captured to obtain optical sections at high spatial resolution, consisting of 10–15 planes with step intervals of 0.3 μm for liver and 4 μm for spinal cord.

For NMJ imaging, fluorescence acquisition was performed using an Olympus spinSR confocal microscope with a 20× objective lens. Maximum-intensity projection images were generated from z-stacks using Fiji (ImageJ) software for enhanced visualization. Additionally, H&E-stained sections of gastrocnemius muscle were digitized using the PANNORAMIC 250 Flash III slide scanner with a 10× objective.

Motoneuron Quantification

Motoneuron analysis was conducted using QuPath and Imaris software. TIFF images were first imported into QuPath, where regions of interest (ROIs) were manually delineated. Nuclei within each ROI were identified in the DAPI channel using the built-in “Cell Detection” function to generate initial detection outputs. These detections were further classified using the “Classify” tool, with parameters optimized to accurately distinguish ChAT-positive and NeuN-positive motoneurons. The classifications were cross-validated through manual inspection in Fiji to ensure counting accuracy.

Quantification of Glial and Human SOD1 Signal Intensity

Fluorescence intensity was quantified using ImageJ software. Microscopy images were first imported and converted to 8-bit format to standardize pixel intensity values. For multi-channel datasets, individual channels were separated to isolate specific fluorescent signals. ROIs were delineated based on fluorescence distribution. Intensity thresholds were then carefully adjusted relative to background intensity to enhance measurement accuracy. The "Area" and "Integrated Density" within these ROIs were measured to obtain quantitative values for fluorescence intensity.

Quantification of Neuromuscular Junctions (NMJs)

Z-stack images of NMJs were acquired and processed using ImageJ as previously described.[52] Endplates were classified as innervated if they exhibited co-localization of BTX and NF signals. Conversely, endplates showing only BTX staining without an associated NF signal were classified as denervated.

Cross-sectional area (CSA) of Muscle

CSA of the gastrocnemius muscle was quantified using *Fiji* software. Muscle fibers were first automatically detected using the built-in segmentation tools, followed by manual correction to ensure accurate boundary delineation. The CSA of individual fibers was then calculated using the "Analyze Particles" function. For each mouse, a minimum of 1,000 fibers was analyzed, and the mean CSA was used for subsequent statistical evaluation.

Statistical Analyses

Data that followed a normal distribution were analyzed using the unpaired Student's t-test for comparisons between two groups. For comparisons among multiple groups or across time points, ANOVA was applied as appropriate. Survival data were analyzed using the Kaplan–Meier method, and group comparisons were made with the log-rank test. Normally distributed continuous data are presented as mean ± standard deviation (SD). Significance levels were defined as follows: $P < 0.05$, $*P < 0.01$, $**P < 0.001$, and $***P < 0.0001$. The number of replicates per experiment is provided in the corresponding figure legends. All analyses were conducted using GraphPad Prism 7 (GraphPad Software, San Diego, CA, USA).

Figures

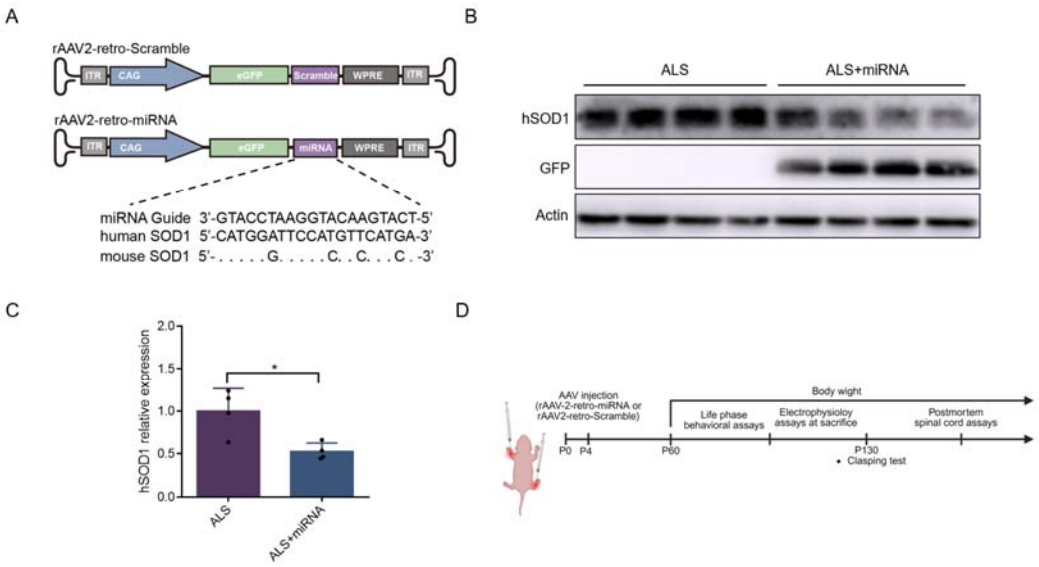

Figure 1. Design and *in vivo* validation of miRNA-hSOD1, an artificial miRNA targeting human SOD1.

(A) Schematic of the AAV vector expressing miRNA-hSOD1. The artificial miRNA was designed with perfect complementarity to human SOD1 and based on the backbone of cellular miR-30a. A

scrambled miRNA that does not target any known gene product was used as a negative control. WPRE: woodchuck hepatitis post-transcriptional regulatory element; ITR: inverted terminal repeat. (B) Western blot analysis of human SOD1 protein expression in spinal cord tissues from rAAV2-retro-Scramble-treated, or rAAV2-retro-miRNA-treated ALS mice. (C) Quantification of human SOD1 suppression in spinal cord tissues. Data are presented as means ± SD, n=4 mice per group. Student's t-test. *P < 0.05. (D) Schematic overview of the experimental timeline and analytical approaches used for ante-mortem and post-mortem evaluations.

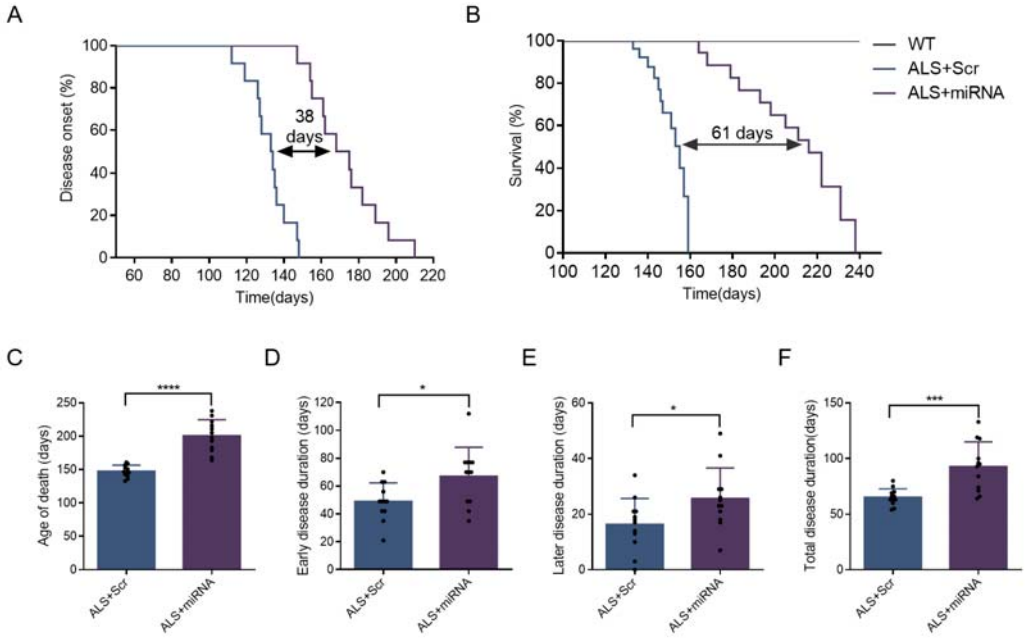

Figure 2. Intramuscular delivery of rAAV2-retro-miRNA delays paralysis, prolongs disease progression, and improves survival in neonatal *SOD1*^{G93A} mice.

(A) Kaplan-Meier curves showing disease onset, defined as a 10% decrease from peak body weight, in rAAV2-retro-miRNA-treated and rAAV2-retro-Scramble-treated *SOD1*^{G93A} mice. Differences were using the log-rank (Mantel-Cox) test. (B) Kaplan-Meier survival curves of rAAV2-retro-miRNA-treated and rAAV2-retro-Scramble-treated *SOD1*^{G93A} mice. Differences were assessed with the log-rank (Mantel-Cox) test. (C) Quantification of median survival in rAAV2-retro-miRNA-treated and rAAV2-retro-Scramble-treated *SOD1*^{G93A} mice. Data represent means ± SD. Student's t-test. (D) Early disease duration in miRNA-treated and scramble-treated *SOD1*^{G93A} mice. Data represent means ± SD, Student's test. (E) Disease duration in rAAV2-retro-miRNA-treated and rAAV2-retro-Scramble-treated *SOD1*^{G93A} mice. Data represent means ± SD, Student's t-test. (F) Total disease duration in miRNA-treated and scramble-treated *SOD1*^{G93A} mice. Data represent means ± SD, Student's t-test; n = 12 mice per group. *P < 0.05, ***P < 0.001, ****P < 0.0001.

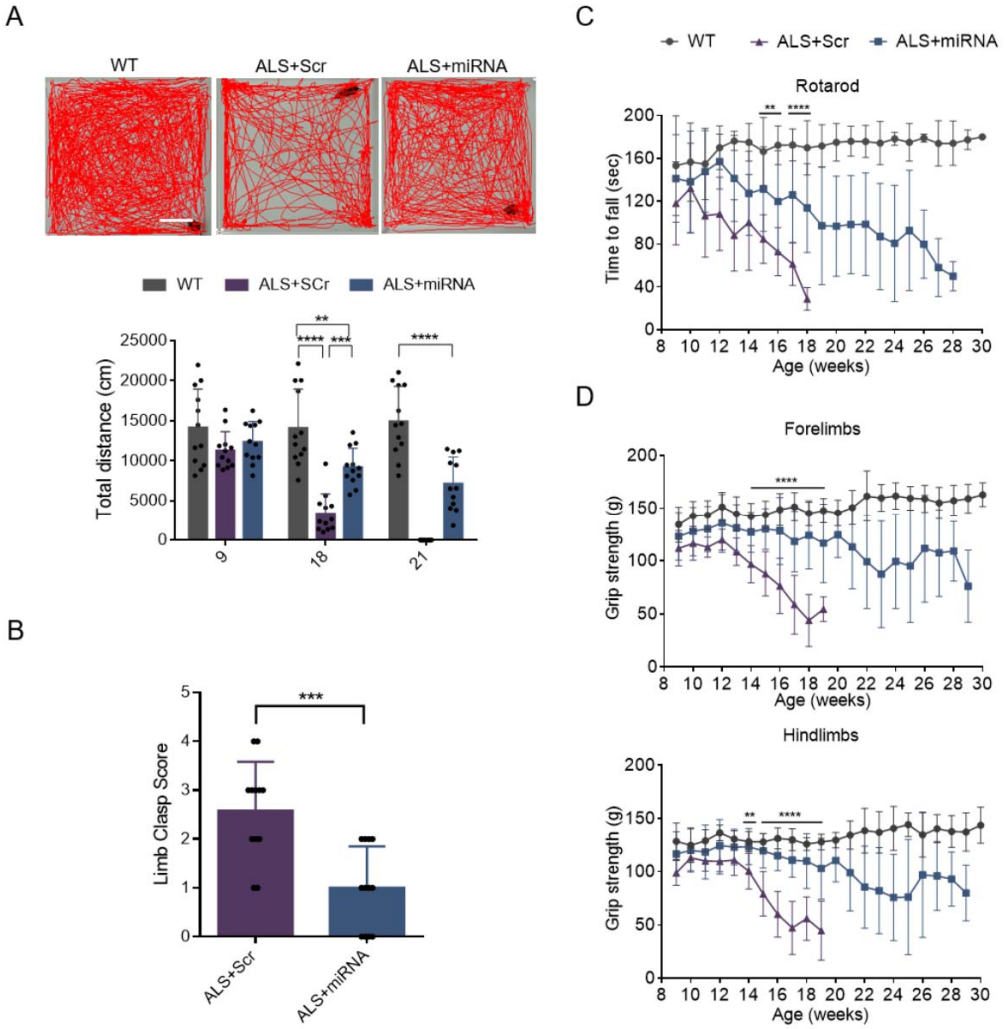

Figure 3. Intramuscular delivery of rAAV2-retro- miRNA leads to long-term preservation of motor function in neonatal *SOD1*^{G93A}mice.

(A) Open-field motor activity, measured as total distance traveled per hour, in WT, rAAV2-retro-Scramble-treated, and rAAV2-retro-miRNA-treated ALS mice. Scale bar, 10 cm. ANOVA with Tukey's post hoc test. (B) Limb clasping score in WT, rAAV2-retro-Scramble-treated, and rAAV2-retro-miRNA-treated ALS mice. Student's t-test. $^{**}P < 0.01$, $^{***}P < 0.001$, $^{****}P < 0.0001$. (C) Rotarod performance of WT, rAAV2-retro-Scramble-treated, and rAAV2-retro-miRNA-treated ALS mice. ANOVA with Tukey's post hoc test. (D) Forelimb and hindlimb grip strength in WT, rAAV2-retro-Scramble-treated, and rAAV2-retro-miRNA-treated ALS mice. ANOVA with Tukey's post hoc test. Data represent mean ± SD ; n = 12 mice per group. $^{**}P < 0.01$, $^{***}P < 0.001$, $^{****}P < 0.0001$ for the comparison between rAAV2-retro-Scramble-treated and rAAV2-retro-miRNA-treated groups

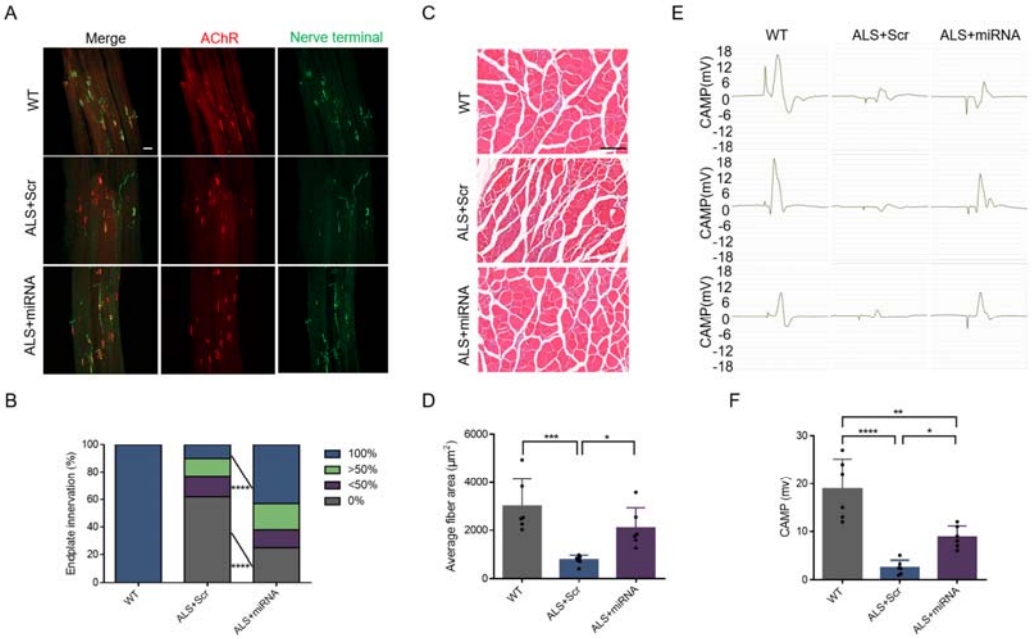

Figure 4. Intramuscular delivery of rAAV2-retro-miRNA preserves neuromuscular junctions, muscle fiber integrity, and motor function in neonatal *SOD1*^{G93A} mice.

(A) Representative immunofluorescence images of gastrocnemius muscles from WT, rAAV2-retro-Scramble-treated, or rAAV2-retro-miRNA-treated ALS mice. Sections were stained with antibodies against neurofilament (NF, presynaptic marker) and α-bungarotoxin (α-BTX, postsynaptic acetylcholine receptor marker). Scale bar, 50 μm. (B) Quantification of neuromuscular junction (NMJ) innervation status, categorized as fully innervated (100%), partially innervated, or fully denervated (0%). Student's t-test. (C) Representative H&E-stained sections of gastrocnemius muscle. Scale bar: 150 μm. (D) Mean cross-sectional area (CSA) of muscle fibers. ANOVA with Tukey's post hoc test. (E) Representative compound muscle action potential (CMAP) recordings from wild-type non-transgenic (left), rAAV2-retro–Scramble-treated (middle), and rAAV2-retro-miRNA-treated *SOD1*^{G93A} mice (right). (F) Quantitative analysis of CMAP amplitudes. ANOVA with Tukey's post hoc test. Data represent mean ± SD, n=6 mice per group. *$P < 0.05$, **$P < 0.01$, ***$P < 0.001$****$P < 0.0001$.

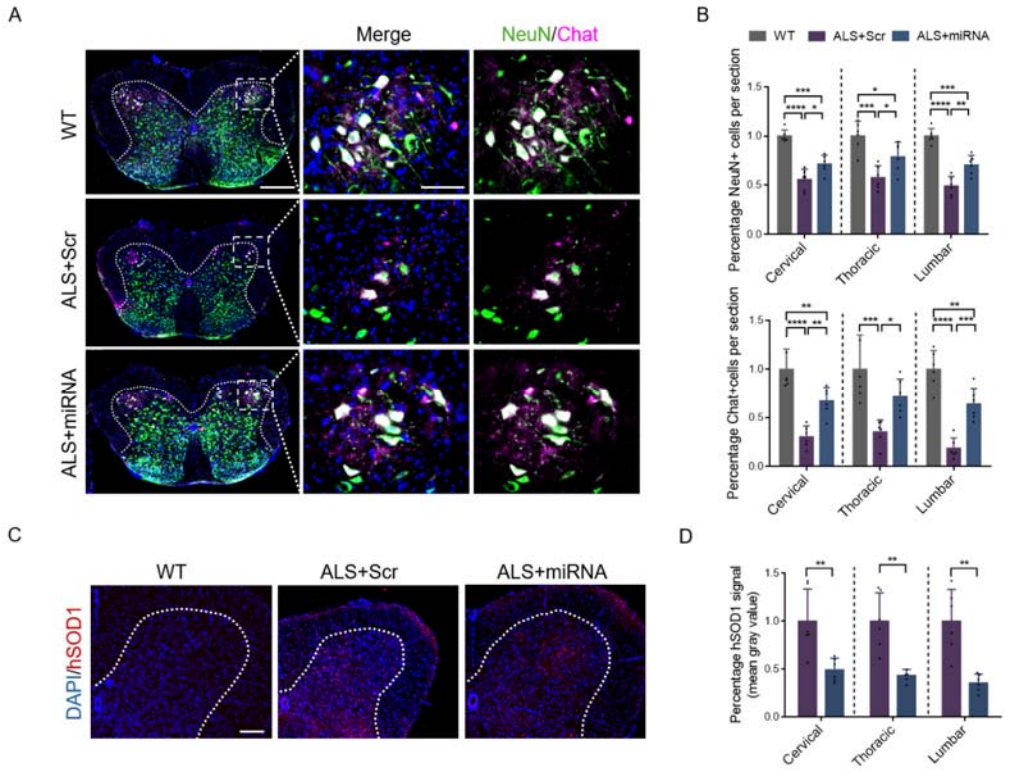

Figure 5. Intramuscular delivery of rAAV2-retro-miRNA preserves α-motor neurons and reduces SOD1 protein accumulation in *SOD1*^{G}mice.

(A) Representative immunofluorescence images of lumbar spinal cord sections from WT, rAAV2-retro-Scramble-treated, and rAAV2-retro-miRNA-treated ALS mice at day 130. Staining markers: NeuN (green), choline acetyltransferase (ChAT, carmine). Nuclei are counterstained with DAPI (blue). Scale bar, 400 μm(left) or 100 μm(right). (B) Quantification of α-motor neurons and NeuN^{+} neurons in cervical, thoracic, and lumbar spinal cord regions. ANOVA with Tukey's post hoc test. (C) Representative images of hSOD1 immunostaining in lumbar spinal cord sections from WT, rAAV2-retro-Scramble-treated, and rAAV2-retro-miRNA-treated ALS mice on day 130. Nuclei are labeled with DAPI (blue); hSOD1 is shown in red. Scale bar, 200 μm. (D) Quantitative analysis of hSOD1 expression levels in cervical, thoracic, and lumbar spinal cord regions. Student's t-test. Data represent mean ± SD，n=6 mice per group. *P < 0.05, **P< 0.01, ***P < 0.001, ****P < 0.0001.

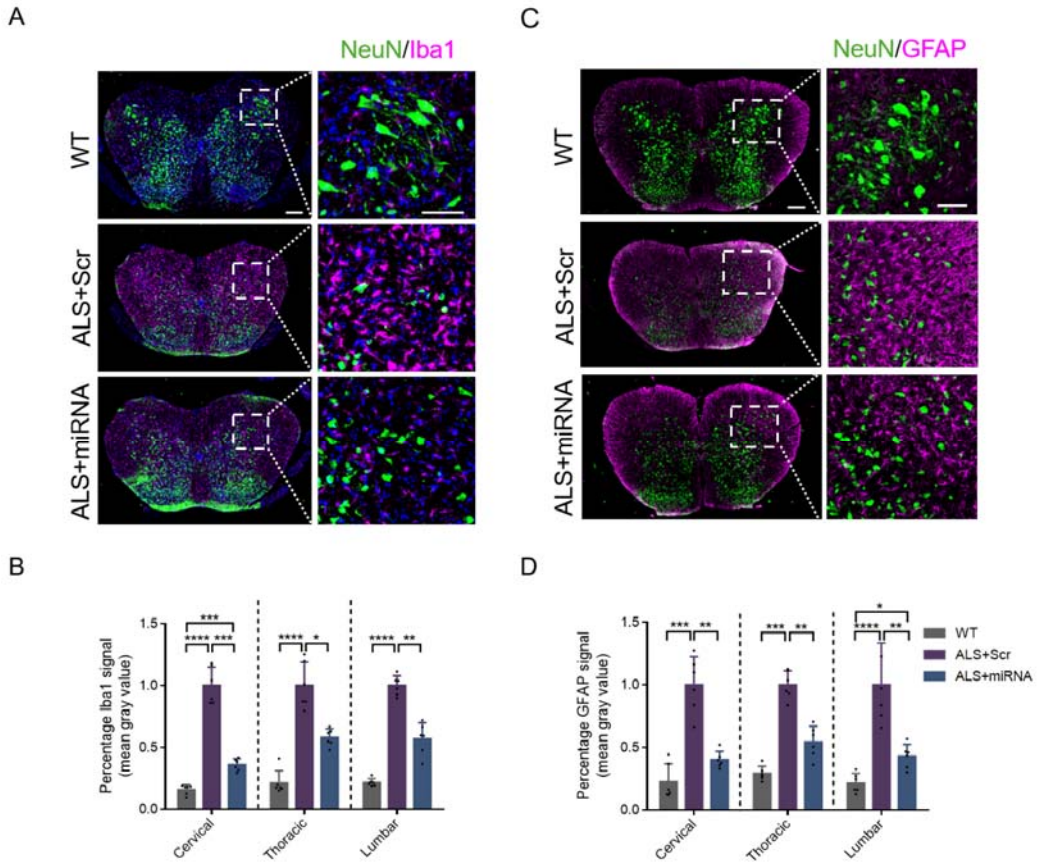

Figure 6. Intramuscular delivery of rAAV2-retro-miRNA attenuates neuroinflammation in *SOD1* ^{G93A} mice.

(A) Representative immunofluorescence images of Iba1^{+} microglia in lumbar spinal cord sections from WT, rAAV2-retro-Scramble-treated, and rAAV2-retro-miRNA-treated ALS mice. Scale bars, 200 µm (left) or 100 µm (right). (B) Quantification of Iba1 fluorescence intensity in the gray matter of wild-type (WT) and treated mice. (C) Representative immunofluorescence images of GFAP^{+} astrocytes in lumbar spinal cord sections from WT, rAAV2-retro-Scramble-treated, and rAAV2-retro-miRNA-treated ALS mice. Scale bars, 200 µm (left) or 100 µm (right). (D) Quantification of GFAP fluorescence intensity in the gray matter. Data represent mean ± SD, n=6 mice per group. ANOVA with Tukey's post hoc test. *$P < 0.05$, **$P < 0.01$, ***$P < 0.001$, ****$P < 0.0001$.

Supplementary Figure 1: Artificial miRNA does not affect murine SOD1 mRNA expression *in vitro*.

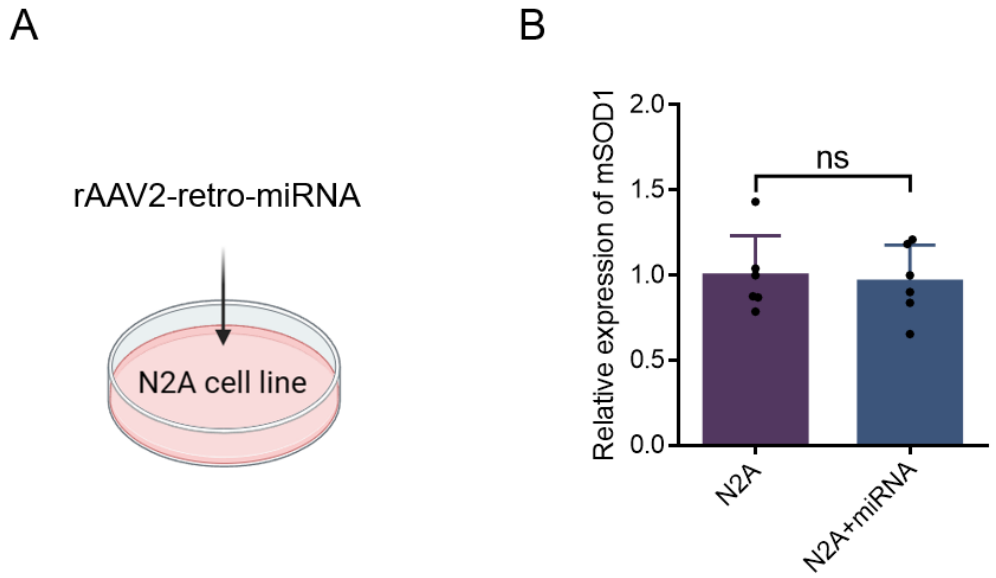

(A) N2A cells were transduced with rAAV2-retro–miRNA for 48 hours, followed by total RNA extraction. (B) Quantification of murine SOD1 (mSOD1) mRNA levels via qPCR, normalized to mGAPDH. Data are presented as individual biological replicates (dots). ns, not significant. Data represent mean ± SD, n=6 per group. Student's t-test.

Supplementary Figure 2: Comparative safety evaluation of rAAV2-retro-shRNA and rAAV2-retro-miRNA in wild-type mice.

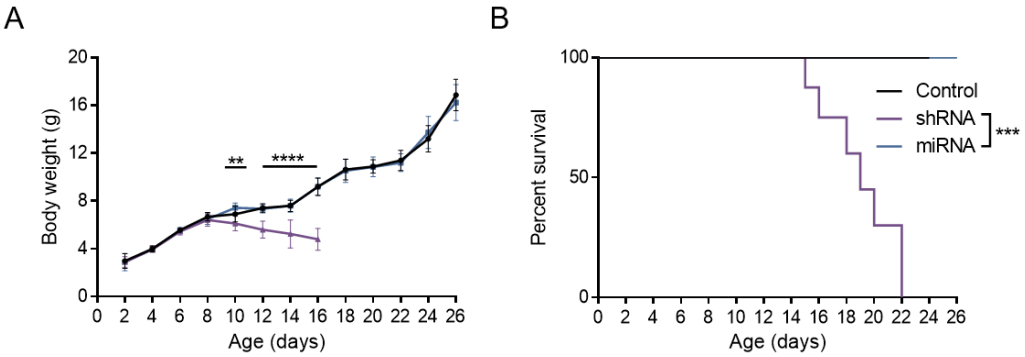

(A) Body weight curves of wild-type mice following intramuscular injection of rAAV2-retro-shRNA or rAAV2-retro-miRNA at postnatal day 4 (P4). n=6 mice per group. ANOVA with Tukey's post hoc test. $^{**}P < 0.01$, $^{****}P < 0.0001$ for the comparison between rAAV2-retro-shRNA-treated and rAAV2-retro-miRNA-treated groups. (B) Kaplan–Meier survival curves of wild-type mice after injection of rAAV2-retro-shRNA or rAAV2-retro-miRNA. Differences were assessed with the log-rank (Mantel–Cox) test. Data are presented as mean ± SD, n=6 mice per group, $^{***}P < 0.001$.

Supplementary Figure 3：Intramuscular delivery of rAAV2-retro attenuates weight loss in *SOD1* ^{G93A} mice.

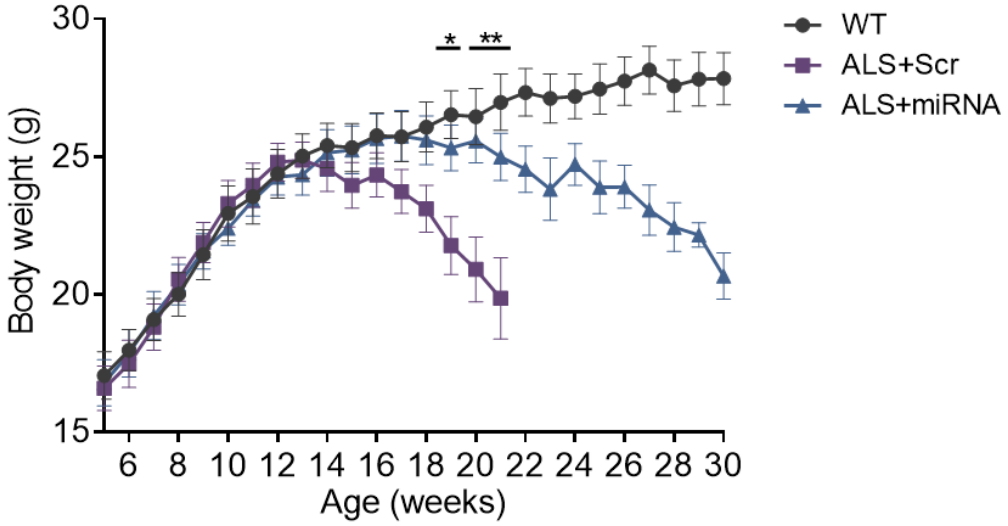

Comparison of the body weight curves of WT, rAAV2-retro-Scramble-treated, and rAAV2-retro-miRNA-treated ALS mice. n=12 mice per group; ANOVA with Tukey's post hoc test. *P < 0.05, **P < 0.01 for the comparison between rAAV2-retro-Scramble-treated and rAAV2-retro-miRNA-treated groups.

Supplementary Figure 4: Representative images and quantitative analysis of the gastrocnemius muscle obtained at day 130 from WT and *SOD1*^{G93A} mice.

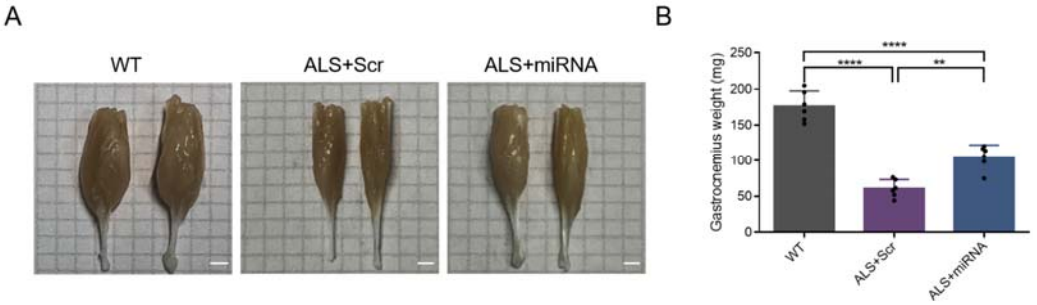

(A) Gastrocnemius muscle sections from P130 WT, rAAV2-retro-Scramble-treated, and rAAV2-retro-miRNA-treated ALS mice. Scale bar, 2mm. (B) Muscle weight quantification. Data represent mean ± SD; n = 6 mice per group. **P< 0.01, ****P < 0.0001; ANOVA with Tukey's post hoc test.

ACKNOWLEDGMENTS

This work was sponsored by the Natural Science Foundation of Shanghai under Grant Nos.

22ZR1414500, 21ZR1407700 (to T.X.).

AUTHOR CONTRIBUTIONS

Conceptualization: W.W., T.X.; data curation: X.G.; supervision: W.W., T.X.; visualization: X.G., T.X.; writing-original draft: X.G., Y.X., W.W., T.X.

DECLARATION OF INTERESTS

The authors declare no competing interests.

REFERENCES

1. Siddique, N., and Siddique, T. (1993). Amyotrophic Lateral Sclerosis Overview. In GeneReviews(®), M.P. Adam, J. Feldman, G.M. Mirzaa, R.A. Pagon, S.E. Wallace, and A. Amemiya, eds. (Seattle (WA): University of Washington, SeattleCopyright © 1993-2025, University of Washington, Seattle. GeneReviews is a registered trademark of the University of Washington, Seattle. All rights reserved.).
2. Mejzini, R., Flynn, L.L., Pitout, I.L., Fletcher, S., Wilton, S.D., and Akkari, P.A. (2019). ALS Genetics, Mechanisms, and Therapeutics: Where Are We Now? Front Neurosci *13*, 1310. 10.3389/fnins.2019.01310.
3. Petrov, D., Mansfield, C., Moussy, A., and Hermine, O. (2017). ALS Clinical Trials Review: 20 Years of Failure. Are We Any Closer to Registering a New Treatment? Front Aging Neurosci *9*, 68. 10.3389/fnagi.2017.00068.
4. Sawada, H. (2017). Clinical efficacy of edaravone for the treatment of amyotrophic lateral sclerosis. Expert Opin Pharmacother *18*, 735-738. 10.1080/14656566.2017.1319937.
5. Cetin, H., Rath, J., Füzi, J., Reichardt, B., Fülöp, G., Koppi, S., Erdler, M., Ransmayr, G., Weber, J., Neumann, K., Hagmann, M., et al. (2015). Epidemiology of amyotrophic lateral sclerosis and effect of riluzole on disease course. Neuroepidemiology *44*, 6-15. 10.1159/000369813.
6. Paganoni, S., Hendrix, S., Dickson, S.P., Knowlton, N., Berry, J.D., Elliott, M.A., Maiser, S., Karam, C., Caress, J.B., Owegi, M.A., Quick, A., et al. (2022). Effect of sodium phenylbutyrate/taurursodiol on tracheostomy/ventilation-free survival and hospitalisation in amyotrophic lateral sclerosis: long-term results from the CENTAUR trial. J Neurol Neurosurg Psychiatry *93*, 871-875. 10.1136/jnnp-2022-329024.
7. Chia, R., Chiò, A., and Traynor, B.J. (2018). Novel genes associated with amyotrophic lateral sclerosis: diagnostic and clinical implications. Lancet Neurol *17*, 94-102. 10.1016/s1474-4422(17)30401-5.
8. Rosen, D.R., Siddique, T., Patterson, D., Figlewicz, D.A., Sapp, P., Hentati, A., Donaldson, D., Goto, J., O'Regan, J.P., Deng, H.X., and et al. (1993). Mutations in Cu/Zn superoxide dismutase gene are associated with familial amyotrophic lateral sclerosis. Nature *362*, 59-62. 10.1038/362059a0.
9. Arai, T., Hasegawa, M., Akiyama, H., Ikeda, K., Nonaka, T., Mori, H., Mann, D., Tsuchiya, K., Yoshida, M., Hashizume, Y., and Oda, T. (2006). TDP-43 is a component of ubiquitin-positive

tau-negative inclusions in frontotemporal lobar degeneration and amyotrophic lateral sclerosis. Biochem Biophys Res Commun *351*, 602-611. 10.1016/j.bbrc.2006.10.093.

10. Neumann, M., Sampathu, D.M., Kwong, L.K., Truax, A.C., Micsenyi, M.C., Chou, T.T., Bruce, J., Schuck, T., Grossman, M., Clark, C.M., McCluskey, L.F., et al. (2006). Ubiquitinated TDP-43 in frontotemporal lobar degeneration and amyotrophic lateral sclerosis. Science *314*, 130-133. 10.1126/science.1134108.
11. Vance, C., Rogelj, B., Hortobágyi, T., De Vos, K.J., Nishimura, A.L., Sreedharan, J., Hu, X., Smith, B., Ruddy, D., Wright, P., Ganesalingam, J., et al. (2009). Mutations in FUS, an RNA processing protein, cause familial amyotrophic lateral sclerosis type 6. Science *323*, 1208-1211. 10.1126/science.1165942.
12. Kwiatkowski, T.J., Jr., Bosco, D.A., Leclerc, A.L., Tamrazian, E., Vanderburg, C.R., Russ, C., Davis, A., Gilchrist, J., Kasarskis, E.J., Munsat, T., Valdmanis, P., et al. (2009). Mutations in the FUS/TLS gene on chromosome 16 cause familial amyotrophic lateral sclerosis. Science *323*, 1205-1208. 10.1126/science.1166066.
13. Renton, A.E., Majounie, E., Waite, A., Simón-Sánchez, J., Rollinson, S., Gibbs, J.R., Schymick, J.C., Laaksovirta, H., van Swieten, J.C., Myllykangas, L., Kalimo, H., et al. (2011). A hexanucleotide repeat expansion in C9ORF72 is the cause of chromosome 9p21-linked ALS-FTD. Neuron *72*, 257-268. 10.1016/j.neuron.2011.09.010.
14. DeJesus-Hernandez, M., Mackenzie, I.R., Boeve, B.F., Boxer, A.L., Baker, M., Rutherford, N.J., Nicholson, A.M., Finch, N.A., Flynn, H., Adamson, J., Kouri, N., et al. (2011). Expanded GGGGCC hexanucleotide repeat in noncoding region of C9ORF72 causes chromosome 9p-linked FTD and ALS. Neuron *72*, 245-256. 10.1016/j.neuron.2011.09.011.
15. Matsumoto, A., Okada, Y., Nakamichi, M., Nakamura, M., Toyama, Y., Sobue, G., Nagai, M., Aoki, M., Itoyama, Y., and Okano, H. (2006). Disease progression of human SOD1 (G93A) transgenic ALS model rats. J Neurosci Res *83*, 119-133. 10.1002/jnr.20708.
16. Kaur, S.J., McKeown, S.R., and Rashid, S. (2016). Mutant SOD1 mediated pathogenesis of Amyotrophic Lateral Sclerosis. Gene *577*, 109-118. 10.1016/j.gene.2015.11.049.
17. van Zundert, B., and Brown, R.H., Jr. (2017). Silencing strategies for therapy of SOD1-mediated ALS. Neurosci Lett *636*, 32-39. 10.1016/j.neulet.2016.07.059.
18. Miller, T., Cudkowicz, M., Shaw, P.J., Andersen, P.M., Atassi, N., Bucelli, R.C., Genge, A., Glass, J., Ladha, S., Ludolph, A.L., Maragakis, N.J., et al. (2020). Phase 1-2 Trial of Antisense Oligonucleotide Tofersen for SOD1 ALS. N Engl J Med *383*, 109-119. 10.1056/NEJMoa2003715.
19. Blair, H.A. (2023). Tofersen: First Approval. Drugs *83*, 1039-1043. 10.1007/s40265-023-01904-6.
20. Rocco, M.T., Akhter, A.S., Ehrlich, D.J., Scott, G.C., Lungu, C., Munjal, V., Aquino, A., Lonser, R.R., Fiandaca, M.S., Hallett, M., Heiss, J.D., et al. (2022). Long-term safety of MRI-guided administration of AAV2-GDNF and gadoteridol in the putamen of individuals with Parkinson's disease. Mol Ther *30*, 3632-3638. 10.1016/j.ymthe.2022.08.003.
21. Ling, Q., Herstine, J.A., Bradbury, A., and Gray, S.J. (2023). AAV-based in vivo gene therapy for neurological disorders. Nat Rev Drug Discov *22*, 789-806. 10.1038/s41573-023-00766-7.
22. Boudreau, R.L., Martins, I., and Davidson, B.L. (2009). Artificial microRNAs as siRNA shuttles: improved safety as compared to shRNAs in vitro and in vivo. Mol Ther *17*, 169-175. 10.1038/mt.2008.231.

23. McBride, J.L., Boudreau, R.L., Harper, S.Q., Staber, P.D., Monteys, A.M., Martins, I., Gilmore, B.L., Burstein, H., Peluso, R.W., Polisky, B., Carter, B.J., et al. (2008). Artificial miRNAs mitigate shRNA-mediated toxicity in the brain: implications for the therapeutic development of RNAi. Proc Natl Acad Sci U S A *105*, 5868-5873. 10.1073/pnas.0801775105.
24. Kaspar, B.K., Lladó, J., Sherkat, N., Rothstein, J.D., and Gage, F.H. (2003). Retrograde viral delivery of IGF-1 prolongs survival in a mouse ALS model. Science *301*, 839-842. 10.1126/science.1086137.
25. Kaspar, B.K., Frost, L.M., Christian, L., Umapathi, P., and Gage, F.H. (2005). Synergy of insulin-like growth factor-1 and exercise in amyotrophic lateral sclerosis. Ann Neurol *57*, 649-655. 10.1002/ana.20451.
26. Allodi, I., Comley, L., Nichterwitz, S., Nizzardo, M., Simone, C., Benitez, J.A., Cao, M., Corti, S., and Hedlund, E. (2016). Differential neuronal vulnerability identifies IGF-2 as a protective factor in ALS. Sci Rep *6*, 25960. 10.1038/srep25960.
27. Lin, H., Hu, H., Duan, W., Liu, Y., Tan, G., Li, Z., Liu, Y., Deng, B., Song, X., Wang, W., Wen, D., et al. (2018). Intramuscular Delivery of scAAV9-hIGF1 Prolongs Survival in the hSOD1(G93A) ALS Mouse Model via Upregulation of D-Amino Acid Oxidase. Mol Neurobiol *55*, 682-695. 10.1007/s12035-016-0335-z.
28. Lee, S.H., Lee, N., Kim, S., Lee, J., Choi, W., Yu, S.S., Kim, J.H., and Kim, S. (2019). Intramuscular delivery of HGF-expressing recombinant AAV improves muscle integrity and alleviates neurological symptoms in the nerve crush and SOD1-G93A transgenic mouse models. Biochem Biophys Res Commun *517*, 452-457. 10.1016/j.bbrc.2019.07.105.
29. Chen, Z., Fan, G., Li, A., Yuan, J., and Xu, T. (2020). rAAV2-Retro Enables Extensive and High-Efficient Transduction of Lower Motor Neurons following Intramuscular Injection. Mol Ther Methods Clin Dev *17*, 21-33. 10.1016/j.omtm.2019.11.006.
30. Gurney, M.E., Pu, H., Chiu, A.Y., Dal Canto, M.C., Polchow, C.Y., Alexander, D.D., Caliendo, J., Hentati, A., Kwon, Y.W., Deng, H.X., and et al. (1994). Motor neuron degeneration in mice that express a human Cu,Zn superoxide dismutase mutation. Science *264*, 1772-1775. 10.1126/science.8209258.
31. Chen, S.K., Hawley, Z.C.E., Zavodszky, M.I., Hana, S., Ferretti, D., Grubor, B., Hawes, M., Xu, S., Hamann, S., Marsh, G., Cullen, P., et al. (2023). Efficacy and safety of a SOD1-targeting artificial miRNA delivered by AAV9 in mice are impacted by miRNA scaffold selection. Mol Ther Nucleic Acids *34*, 102057. 10.1016/j.omtn.2023.102057.
32. Biferi, M.G., Cohen-Tannoudji, M., Cappelletto, A., Giroux, B., Roda, M., Astord, S., Marais, T., Bos, C., Voit, T., Ferry, A., and Barkats, M. (2017). A New AAV10-U7-Mediated Gene Therapy Prolongs Survival and Restores Function in an ALS Mouse Model. Mol Ther *25*, 2038-2052. 10.1016/j.ymthe.2017.05.017.
33. Eisen, A., Kiernan, M., Mitsumoto, H., and Swash, M. (2014). Amyotrophic lateral sclerosis: a long preclinical period? J Neurol Neurosurg Psychiatry *85*, 1232-1238. 10.1136/jnnp-2013-307135.
34. Salvany, S., Casanovas, A., Piedrafita, L., Tarabal, O., Hernández, S., Calderó, J., and Esquerda, J.E. (2021). Microglial recruitment and mechanisms involved in the disruption of afferent synaptic terminals on spinal cord motor neurons after acute peripheral nerve injury. Glia *69*, 1216-1240. 10.1002/glia.23959.
35. Yu, J.C., Khodadadi, H., Malik, A., Davidson, B., Salles É, D.S.L., Bhatia, J., Hale, V.L., and

Baban, B. (2018). Innate Immunity of Neonates and Infants. Front Immunol *9*, 1759. 10.3389/fimmu.2018.01759.

36. Foust, K.D., Nurre, E., Montgomery, C.L., Hernandez, A., Chan, C.M., and Kaspar, B.K. (2009). Intravascular AAV9 preferentially targets neonatal neurons and adult astrocytes. Nat Biotechnol *27*, 59-65. 10.1038/nbt.1515.
37. Peggion, C., Scalcon, V., Massimino, M.L., Nies, K., Lopreiato, R., Rigobello, M.P., and Bertoli, A. (2022). SOD1 in ALS: Taking Stock in Pathogenic Mechanisms and the Role of Glial and Muscle Cells. Antioxidants (Basel) *11*. 10.3390/antiox11040614.
38. Meijboom, K.E., and Brown, R.H. (2022). Approaches to Gene Modulation Therapy for ALS. Neurotherapeutics *19*, 1159-1179. 10.1007/s13311-022-01285-w.
39. Hinderer, C., Katz, N., Dyer, C., Goode, T., Johansson, J., Bell, P., Richman, L., Buza, E., and Wilson, J.M. (2020). Translational Feasibility of Lumbar Puncture for Intrathecal AAV Administration. Mol Ther Methods Clin Dev *17*, 969-974. 10.1016/j.omtm.2020.04.012.
40. Tortelli, R., Conforti, F.L., Cortese, R., D'Errico, E., Distaso, E., Mazzei, R., Ungaro, C., Magariello, A., Gambardella, A., Logroscino, G., and Simone, I.L. (2013). Amyotrophic lateral sclerosis: a new missense mutation in the SOD1 gene. Neurobiol Aging *34*, 1709.e1703-1705. 10.1016/j.neurobiolaging.2012.10.027.
41. Chattopadhyay, M., and Valentine, J.S. (2009). Aggregation of copper-zinc superoxide dismutase in familial and sporadic ALS. Antioxid Redox Signal *11*, 1603-1614. 10.1089/ars.2009.2536.
42. Paré, B., Lehmann, M., Beaudin, M., Nordström, U., Saikali, S., Julien, J.P., Gilthorpe, J.D., Marklund, S.L., Cashman, N.R., Andersen, P.M., Forsberg, K., et al. (2018). Misfolded SOD1 pathology in sporadic Amyotrophic Lateral Sclerosis. Sci Rep *8*, 14223. 10.1038/s41598-018-31773-z.
43. Berdyński, M., Miszta, P., Safranow, K., Andersen, P.M., Morita, M., Filipek, S., Żekanowski, C., and Kuźma-Kozakiewicz, M. (2022). SOD1 mutations associated with amyotrophic lateral sclerosis analysis of variant severity. Sci Rep *12*, 103. 10.1038/s41598-021-03891-8.
44. Baird, M.C., Likhite, S.B., Vetter, T.A., Caporale, J.R., Girard, H.B., Roussel, F.S., Howard, A.E., Schwartz, M.K., Reed, A.R., Kaleem, A., Zhang, X., et al. (2024). Combination AAV therapy with galectin-1 and SOD1 downregulation demonstrates superior therapeutic effect in a severe ALS mouse model. Mol Ther Methods Clin Dev *32*, 101312. 10.1016/j.omtm.2024.101312.
45. Rothstein, J.D. (2009). Current hypotheses for the underlying biology of amyotrophic lateral sclerosis. Ann Neurol *65 Suppl 1*, S3-9. 10.1002/ana.21543.
46. Saccon, R.A., Bunton-Stasyshyn, R.K., Fisher, E.M., and Fratta, P. (2013). Is SOD1 loss of function involved in amyotrophic lateral sclerosis? Brain *136*, 2342-2358. 10.1093/brain/awt097.
47. Amado, D.A., and Davidson, B.L. (2021). Gene therapy for ALS: A review. Mol Ther *29*, 3345-3358. 10.1016/j.ymthe.2021.04.008.
48. Abati, E., Bresolin, N., Comi, G., and Corti, S. (2020). Silence superoxide dismutase 1 (SOD1): a promising therapeutic target for amyotrophic lateral sclerosis (ALS). Expert Opin Ther Targets *24*, 295-310. 10.1080/14728222.2020.1738390.
49. Shiryaeva, O., Tolochko, C., Alekseeva, T., and Dyachuk, V. (2025). Targets and Gene Therapy of ALS (Part 1). Int J Mol Sci *26*. 10.3390/ijms26094063.

50. Grimm, D., Streetz, K.L., Jopling, C.L., Storm, T.A., Pandey, K., Davis, C.R., Marion, P., Salazar, F., and Kay, M.A. (2006). Fatality in mice due to oversaturation of cellular microRNA/short hairpin RNA pathways. Nature *441*, 537-541. 10.1038/nature04791.
51. Course, M.M., Gudsnuk, K., Desai, N., Chamberlain, J.R., and Valdmanis, P.N. (2020). Endogenous MicroRNA Competition as a Mechanism of shRNA-Induced Cardiotoxicity. Mol Ther Nucleic Acids *19*, 572-580. 10.1016/j.omtn.2019.12.007.
52. Cheng, W., Huang, J., Fu, X.Q., Tian, W.Y., Zeng, P.M., Li, Y., and Luo, Z.G. (2023). Intrathecal delivery of AAV-NDNF ameliorates disease progression of ALS mice. Mol Ther *31*, 3277-3289. 10.1016/j.ymthe.2023.09.018.